Supporting Information

On-Demand Detachable Hydrogel Electrodes with Robust Adhesion for Epidermal Electrophysiological Monitoring

Qiaoqiao Fang, Zhiliang Han, Mengyao Guan, Qingxin Ge, Tao Zhang, Huaping Wang*, Shiyan Chen*

State Key Laboratory of Advanced Fiber Materials, College of Materials Science and Engineering, Donghua University, Shanghai 201620, China

E-mail: wanghp@dhu.edu.cn, chensy@dhu.edu.cn

MATERIALS AND METHODS

Materials

N-isopropylacrylamide (NIPAAM, 98 %, Shanghai Titan Scientific Co., Ltd.), Acrylic acid (AA, 98 %, Shanghai Titan Scientific Co., Ltd.), tannic acid (TA, 99 %, Shanghai Titan Scientific Co., Ltd.), ferric chloride ($FeCl_3$, 99 %, Shanghai Macklin Biochemical Co., Ltd.), N,N'-methylenebisacrylamide (MBA, 99 %, Shanghai Aladdin Biochemical Technology Co., Ltd.), and ammonium persulfate (APS, 98 %, Sinopharm Chemical Reagent Co., Ltd.). All chemicals were commercially sourced and used without further purification.

Preparation of P(AA-co-NIPAAM) hydrogel

An aqueous solution was first prepared by dissolving 75 mg of tannic acid (TA) and 0.75 mg of $FeCl_3$ in 2 mL of deionized water under vigorous stirring. In a separate beaker, 1 g of NIPAAM and 2 g of AA were dissolved in 5 mL of deionized water, followed by the addition of 8 mg of the crosslinker MBA and 15 mg of the initiator APS. The TA-Fe^{3+} solution was then incorporated into the monomer mixture and stirred until homogeneity was achieved. The resulting precursor solution was poured into a rectangular mold and allowed to gel at ambient temperature within 2 minutes. Hydrogels with varying TA or AA contents were synthesized following an analogous procedure, with detailed formulations provided in Table S1.

Preparation of injected P(AA-co-NIPAAM) hydrogel electrodes

First, a precursor mixed solution containing AA, NIPAAM, TA-Fe^{3+}, MBA, and APS was directly injected onto the target skin area of the volunteer's forearm. After it underwent in situ gelation on the skin surface, the current collector layer (carbon paper, silver paste, and conductive wire) was then gently attached to the surface of the gel.

Characterization of TA-Fe^{3+} complex

UV-visible absorption spectra were recorded using a spectrophotometer (Evolution 201) over a wavelength range of 200-800 nm. Cyclic voltammetry measurements were performed with an electrochemical workstation (CHI660E) to investigate the interactions between TA and Fe^{3+}. Elemental composition and chemical

states were analyzed by X-ray photoelectron spectroscopy (Escalab 250Xi). High-resolution XPS spectra were deconvoluted using Vantage software, with all peaks calibrated relative to the C 1s peak at 284.8 eV. The gelation process of the hydrogel was monitored in real-time using an infrared thermal camera (E86-EST).

Characterization of P(AA-co-NIPAAM) hydrogel

The surface morphology and elemental composition of the hydrogel were examined using scanning electron microscopy with energy-dispersive X-ray spectroscopy (SEM-EDS, GeminiSEM 560). FTIR spectra were acquired on a Nicolet iS50 spectrometer in the wavenumber range of 4000–400 cm^{-1}. Optical transmittance of the hydrogel at 25 ℃ and 45 ℃ was measured by UV-vis spectrophotometry (Evolution 201) between 500-800 nm, with data in the 690-710 nm range representing transmittance at 700 nm. Rheological properties were evaluated using a rotational rheometer (MCR302, Anton Paar). Time-dependent modulus evolution was monitored through dynamic time-sweep experiments at ambient temperature, while temperature-dependent viscoelastic behavior was characterized by temperature-sweep tests from 25 to 60 ℃ for hydrogels with varying AA content. All rheological measurements were conducted at a fixed angular frequency of 6.28 rad/s and 1 % strain.

Mechanical tests

Uniaxial tensile tests were performed using an electronic universal testing machine (Instron 5969) equipped with a 50 N load cell. Rectangular specimens (20 × 15 × 2 mm, length × width × thickness) were stretched at a constant crosshead speed of 100 mm/min under ambient conditions to obtain stress-strain curves, with each condition repeated for at least five independent measurements. Engineering stress was calculated as the applied force divided by the original cross-sectional area, while strain was defined as the deformation length relative to the initial gauge length. Cyclic tensile tests were conducted on identical specimens by loading and unloading for three consecutive cycles at prescribed strains of 25 %, 50 %, 100 %, 200 %, 300 %, 400 %, 500 %, 600 %, 700 %, and 800 %. Fracture toughness was determined based on a reported method comparing notched and unnotched tensile specimens. The fracture energy (Γ) was computed by integrating the area under the stress-strain curve of unnotched samples

from zero strain to the critical strain (ε_c), multiplied by the original gauge length (H) between clamps, according to the following equation:

$$\Gamma = H \int_0^{\varepsilon_c} \sigma \mathrm{d}\varepsilon$$

Adhesion properties

The adhesive properties of the hydrogel to various engineering solid materials (plastics, rubber, aluminum sheets, copper sheets) and hydrated biological tissues (porcine skin, heart, liver, and muscle) were characterized through 180° peel tests and lap-shear tests. Specimens were firmly fixed between two substrates and evaluated using a universal testing system (Instron 5969, 50 N load cell) with over five replicates per condition. Interfacial toughness was derived by dividing the steady-state peeling force by the adhesive sample width, while shear strength was calculated as the maximum force divided by the bonded area. All mechanical tests were conducted at a constant crosshead speed of 100 mm/min.

Biocompatibility assessment

L929 fibroblast cells were cultured in Dulbecco's modified Eagle's medium (DMEM, Gibco) containing 1 % penicillin/streptomycin (Pen/Strep) and 10 % fetal bovine serum (FBS). The cells were cultured at 37 ℃, 95 % humidity and 5 % CO_2. Prior to cell seeding, hydrogel samples were sterilized via 2 hours UV exposure followed by immersion in 75 % ethanol overnight and rinsing with PBS. Cells were seeded at a density of 2×10^4 cells/mL. After 24 hours incubation, cell viability was evaluated using CCK-8 assay: DMEM containing 10 % CCK-8 reagent was added, incubated for 90 minutes, and absorbance was measured at 450 nm. Live/dead staining was performed using a solution of 1/1000 AM and 1/4000 PI incubated for 30 min. Cell viability was visualized using laser scanning confocal microscopy (LSCM, Carl Zeiss LSM710), with images processed via ImageJ software.

Electrophysiological signal recording

Electrocardiogram (ECG) and electromyogram (EMG) signals were recorded on a healthy adult volunteer using a commercially available portable brain-muscle electrical signal module. Each measurement was performed in triplicate to confirm

reproducibility. The P(AA-co-NIPAAM) hydrogel electrode served as the working electrode, positioned on the volunteer's chest and right arm flexor muscle. Reference electrodes were placed at the contralateral chest site and the wrist, while the ground electrode was attached to the ankle. Both the P(AA-co-NIPAAM) hydrogel electrode and the commercial Ag/AgCl electrode used in the tests had a surface area of 1 cm^2. Before each electrode placement, the target skin areas were cleaned with alcohol wipes to ensure consistent surface conditions. Signal-to-noise ratio (SNR) is an important indicator for evaluating signal quality and is typically expressed in decibels (dB). A higher SNR indicates clearer signals and less background interference. Raw signal data were exported without additional filtering, and the SNR calculations were performed directly on the acquired waveforms. Specifically, 3 to 5 motion-artifact-free segments of equal length were selected from stable signal segments, and their RMS value was calculated as V_{signal}. Simultaneously, the same number of equal-length segments were selected from the baseline segment without signal stimulation, and their RMS value was calculated as V_{noise}. The SNR calculation formula is: $SNR = 20 \times lg (V_{Signal}/V_{noise})$.

Table S1. The main components for P(AA-co-NIPAAM) hydrogels.

Materials	NIPAAM (g)	AA(g)	TA (mg)	$FeCl_3$ (mg)	H_2O (mL)	MBA (mg)	APS (mg)
NIPAAM:AA 1:2	1	2	**75**	0.75	7	8	15
NIPAAM:AA 1:1.5	1.2	1.8	75	0.75	7	8	15
NIPAAM:AA 1:2.5	0.86	2.14	75	0.75	7	8	15
TA-25	1	2	**25**	0.75	7	8	15
TA-50	1	2	**50**	0.75	7	8	15

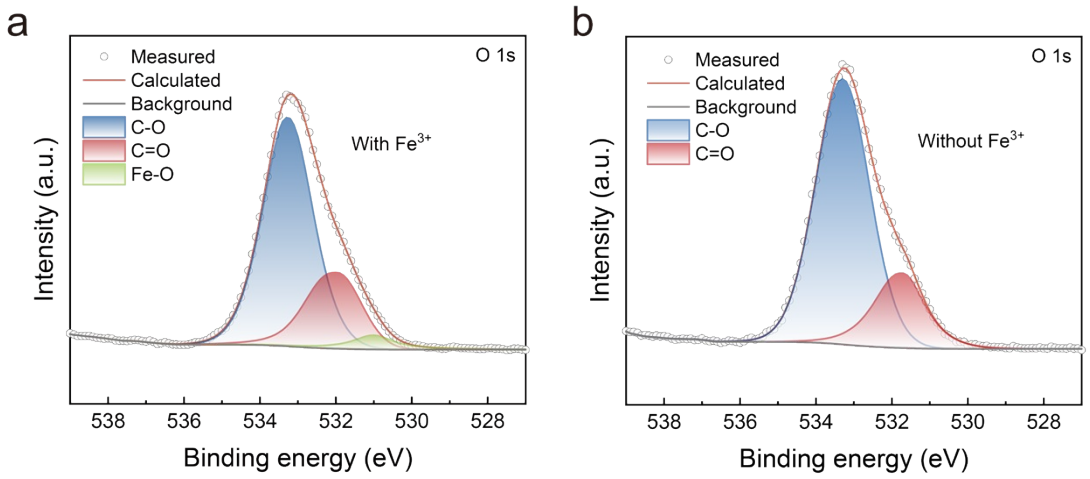

Fig. S1. (a) O 1s XPS spectrum of TA-Fe^{3+} redox pairs, characterizing the redox reaction. (b) XPS spectrum of O 1s for TA.

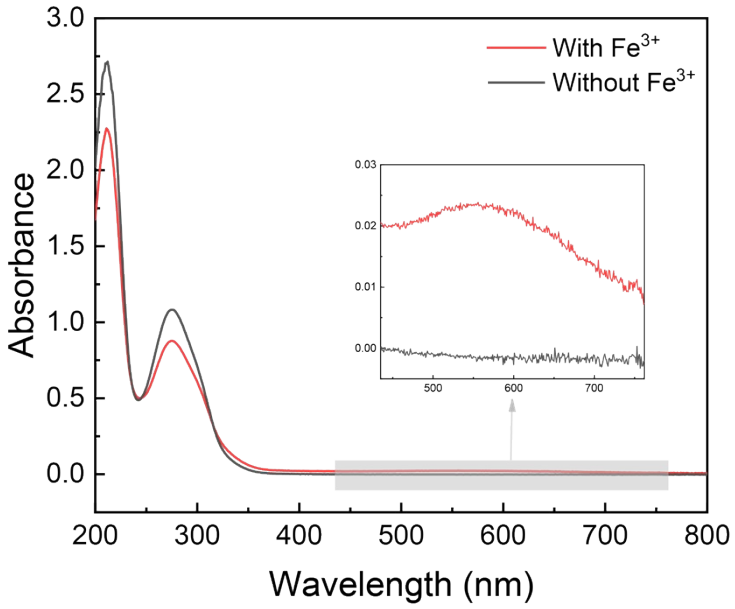

Fig. S2. UV-vis spectra of TA and TA-Fe^{3+}.

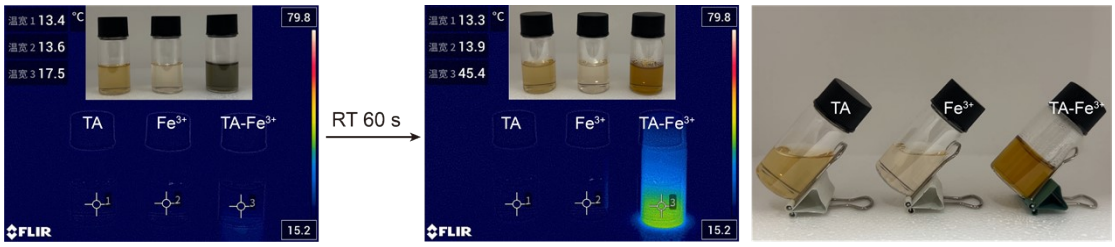

Fig. S3. The sol-gel transition and exothermic process of hydrogels containing TA alone, Fe^{3+} alone, and the TA-Fe^{3+} system.

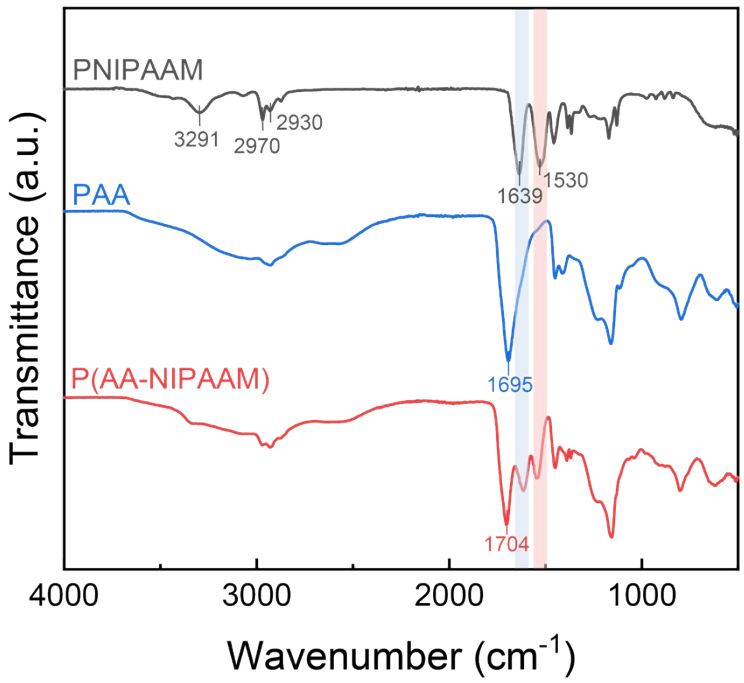

Fig. S4. FTIR spectra of PNIPAAM, PAA and P(AA-co-NIPAAM).

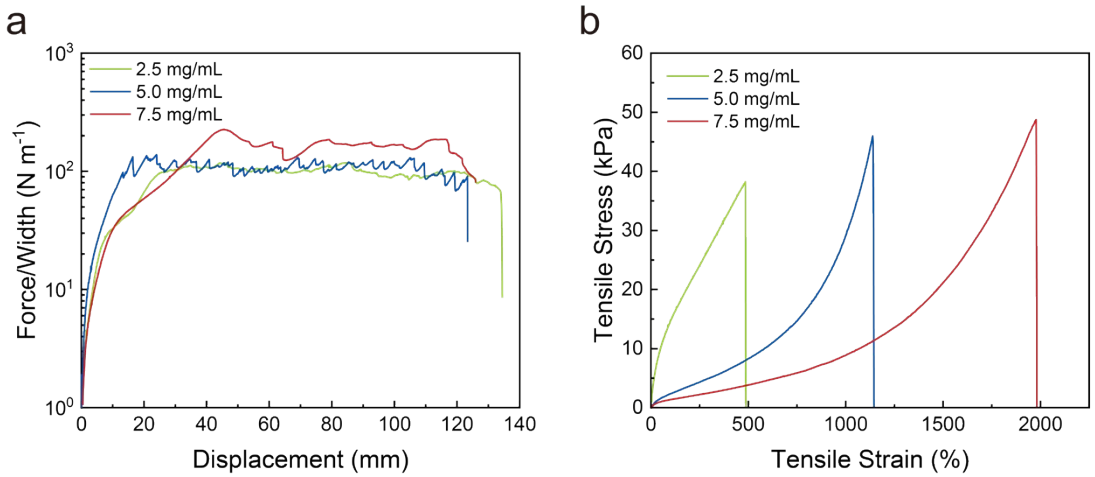

Fig. S5. (a) Force per width versus displacement curves for 180-degree peel tests of P(AA-co-NIPAAM) hydrogels with different TA contents on porcine skin. (b) Tensile stress-strain curves from tensile tests of P(AA-co-NIPAAM) hydrogels with different TA contents.

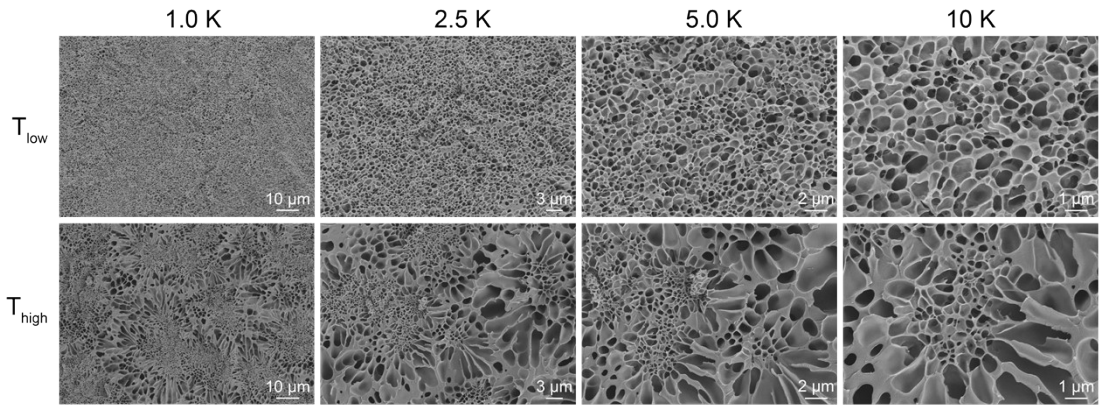

Fig. S6. SEM images of P(AA-co-NIPAAM) hydrogel at different magnifications under varying temperatures.

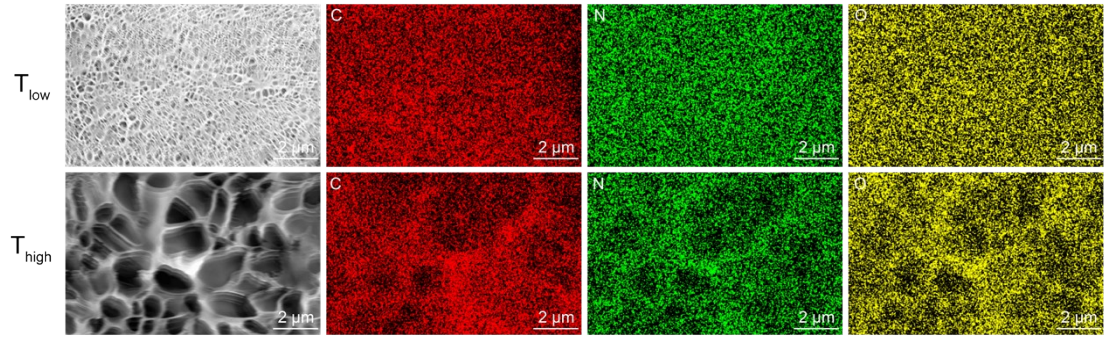

Fig. S7. SEM images and corresponding EDS elemental mapping of P(AA-co-NIPAAM) hydrogel at different temperatures.

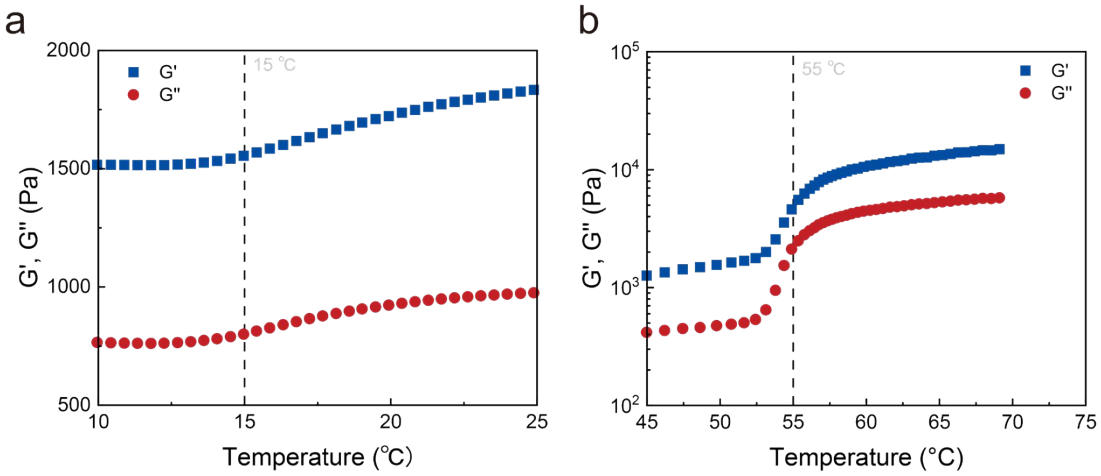

Fig. S8. (a) Variation of storage modulus (G') and loss modulus (G'') with NIPAAM/AA content of 1:1.5. (b) Variation of G' and G'' with NIPAAM/AA content of 1:2.5.

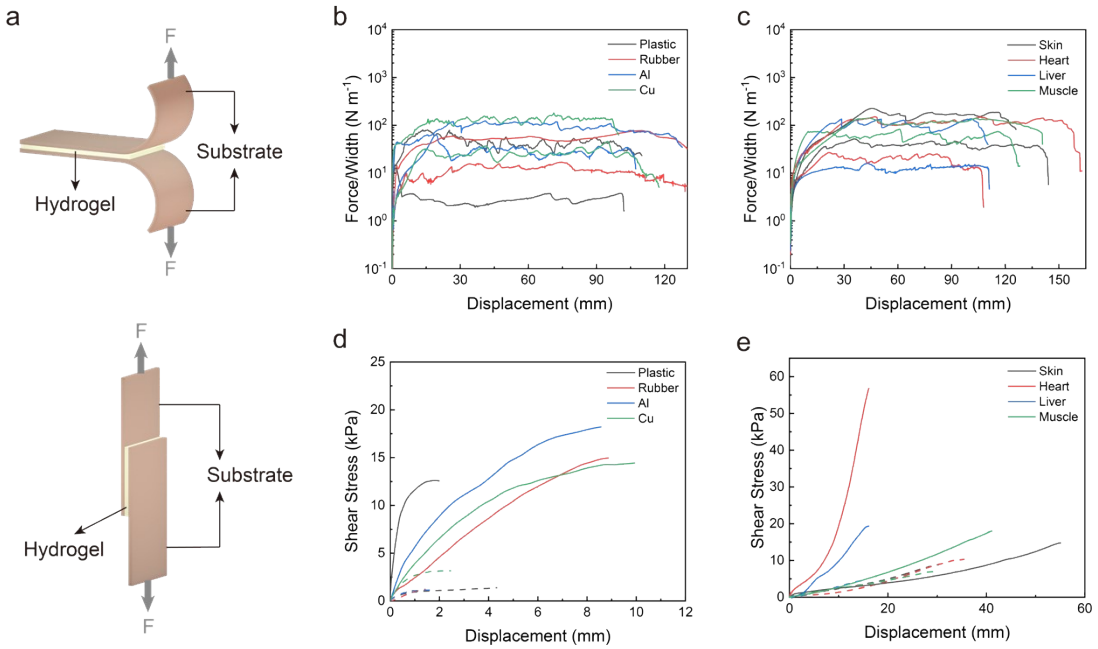

Fig. S9. (a) Schematic diagrams of the 180-degree peel test and lap-shear test. (b) Force per width versus displacement curves from 180-degree peel tests of P(AA-co-NIPAAM) hydrogel on different engineering materials at varying temperatures. (c) Shear stress versus displacement curves from lap-shear tests of P(AA-co-NIPAAM) hydrogel on different engineering materials at varying temperatures. (d) Force per width versus displacement curves from 180-degree peel tests of P(AA-co-NIPAAM) hydrogel on different biological tissues at varying temperatures. (e) Shear stress versus displacement curves from lap-shear tests of P(AA-co-NIPAAM) hydrogel on different biological tissues at varying temperatures.

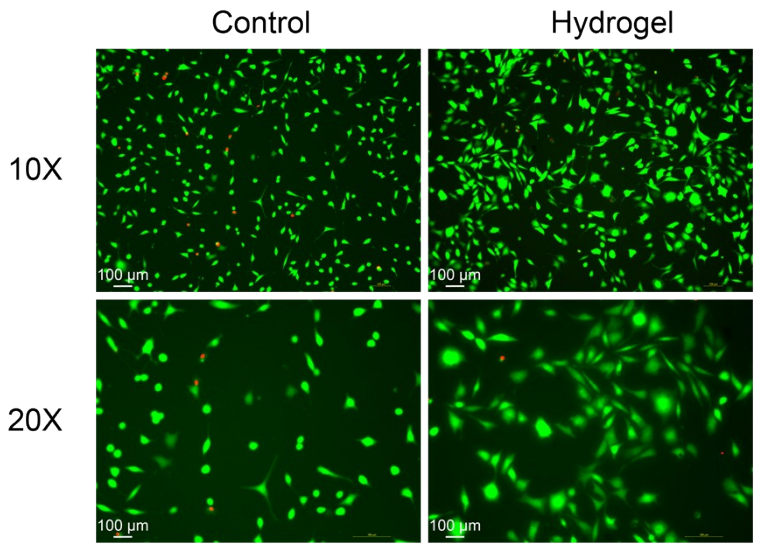

Fig. S10. In vitro biocompatibility of P(AA-co-NIPAAM) hydrogel assessed by live/dead assay of mouse fibroblast cells (L929) after 24 hours of culture.

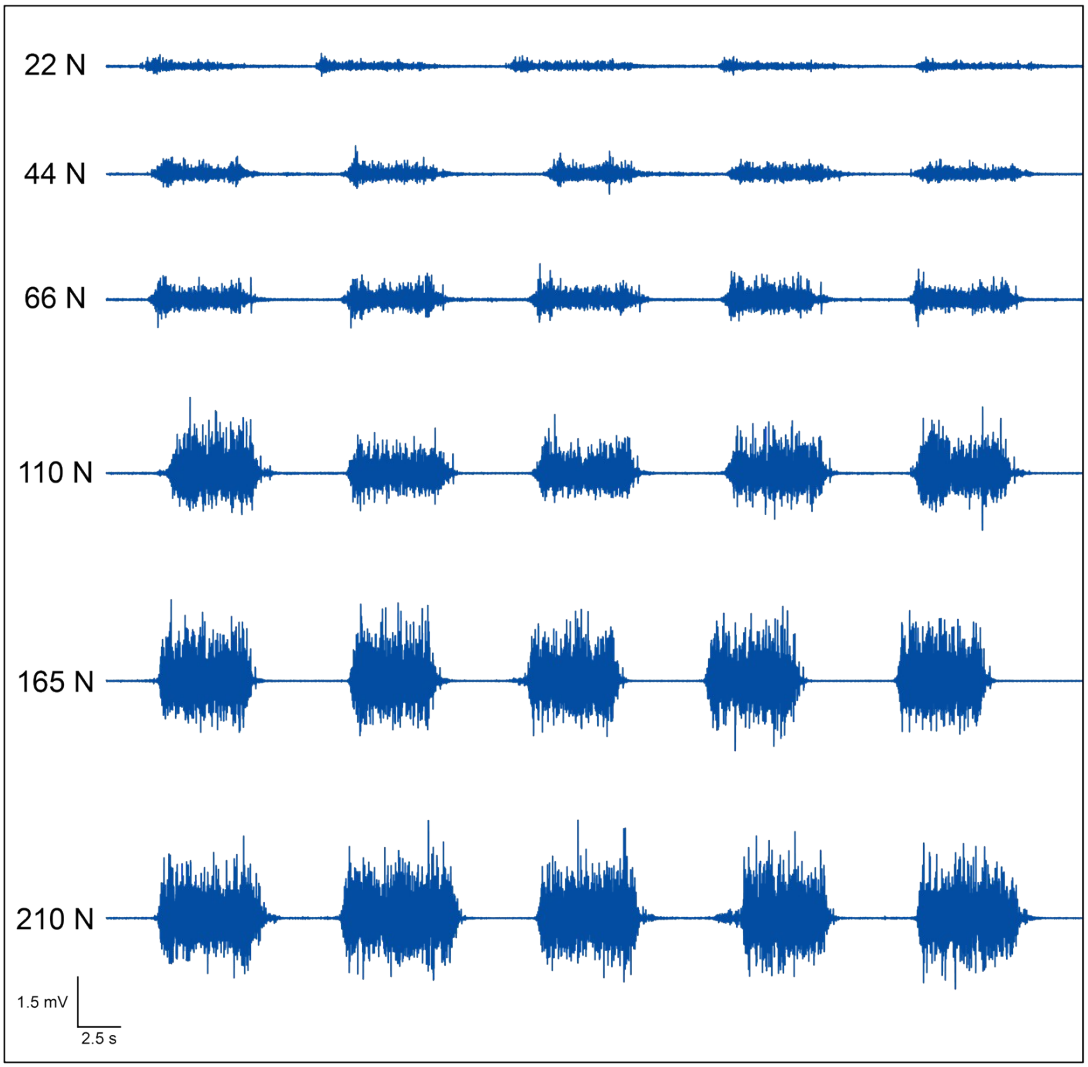

Fig. S11. Electromyography (EMG) signals recorded by P(AA-co-NIPAAM) hydrogel electrodes under different grip strengths.

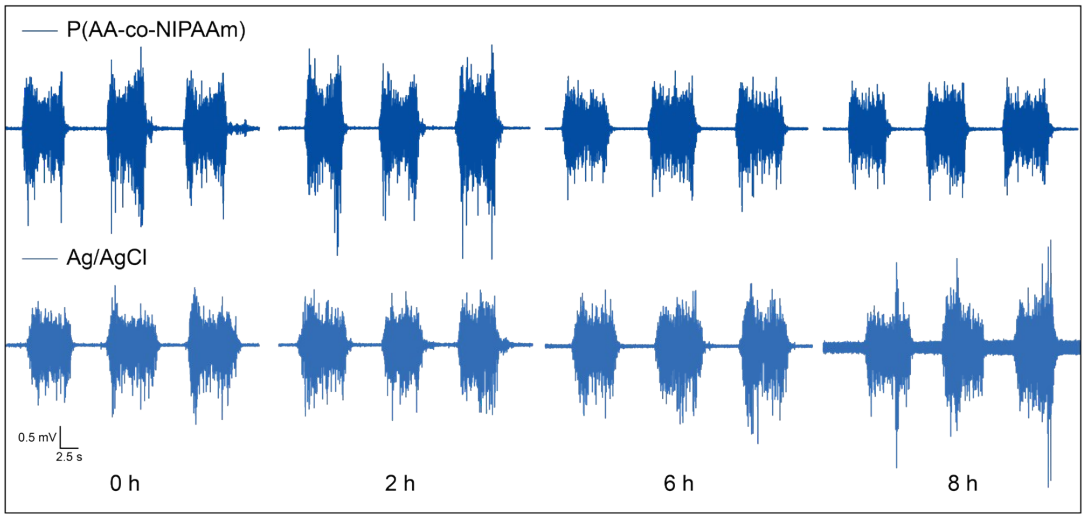

Fig. S12. Electromyography (EMG) signals recorded by P(AA-co-NIPAAM) hydrogel electrodes and commercial Ag/AgCl electrodes during long-term testing at 0, 2, 6, and 8 h.

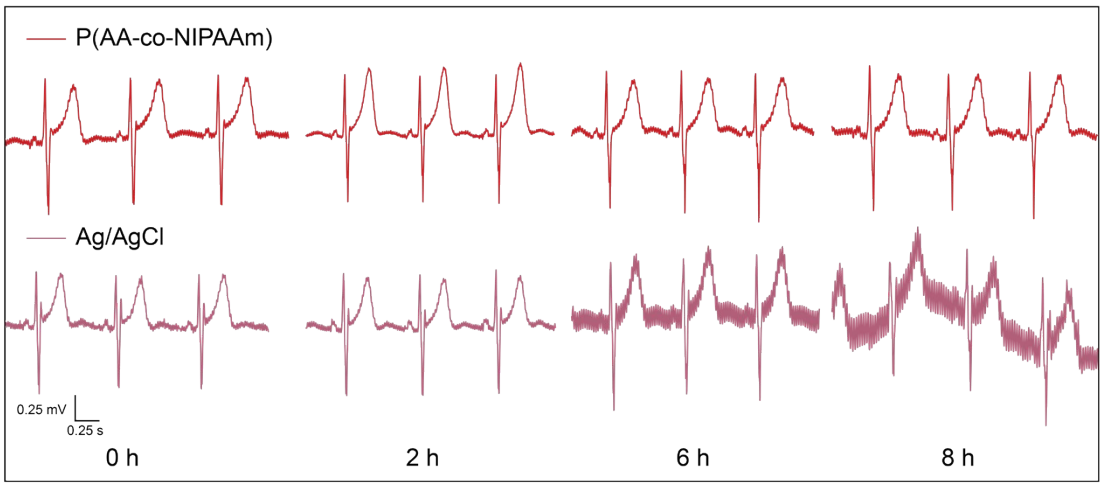

Fig. S13. Electrocardiography (ECG) signals recorded by P(AA-co-NIPAAM) hydrogel electrodes and commercial Ag/AgCl electrodes during long-term testing at 0, 2, 6, and 8 h.